AIAA JOURNAL
Vol. 34, No. 1, January 1996

Actuator with Built-In Viscous Damping for Isolation and Structural Control

T. Tupper Hyde*
Massachusetts Institute of Technology, Cambridge, Massachusetts 02139
and
Eric H. Anderson†
CSA Engineering, Inc., Palo Alto, California 94303

The development and experimental application of an actuator with built-in viscous damping are described. A passive damper was modified to create a novel actuation device for two applications: isolation and structural control. The device uses the same fluid for damping and as a hydraulic lever for a voice coil actuator. For vibration suppression, active enhancement of the inherent passive damping can optimize broadband damping or target certain frequencies. For vibration isolation applications, the passive stiffness can be chosen for small gravity sag and the active control designed to provide reduced mount transmissibility over a broad- or narrow-frequency range. Lumped parameter models capturing structural and fluid effects are presented. Component tests of free stroke, blocked force, and passive complex stiffness are used to update assumed model parameters. The structural damping effectiveness of the new actuator is shown to be that of a typical passive viscous damper and that of an actively damped piezoelectric strut with load cell feedback in a complex truss structure. Open- and closed-loop results are presented for a force isolation application showing an 8-dB passive and a 20-dB active improvement over an undamped mount.

Introduction

PASSIVE means of damping or isolation have proven effective in numerous applications.[1-3] Yet there are some cases where greater performance is demanded, and passive approaches are constrained by fundamental limitations. In these cases, active enhancement of the passive capabilities is an attractive option. Active enhancement implies that when the active system is turned off, or when it fails, the passive capability remains.

The limitations of passive isolation are well known.[1] A low corner frequency of an isolator f_0 improves isolation at the expense of large sag under static loading. For frequencies below $\sqrt{2}f_0$, the isolator amplifies base motion. Amplification is greatest at the mount resonance and for more lightly damped isolators. With passive isolators, narrow-band disturbances are only effectively isolated by introducing additional dynamics (internal resonances) in the isolator.

Active mounts effectively decouple the isolator corner frequency from static sag.[4] The transmissibility can be more easily tailored to emphasize frequency bands containing significant disturbance energy. Narrow-band isolation is readily achieved with an active mount and, if necessary, the band of isolation can track time-varying disturbance frequencies. A combination passive/active mount achieves both the high-frequency attenuation of passive isolation, and the tunability and narrow-band capability of active isolation.

Hybrid passive/active devices are also advantageous for structural damping and control, particularly in systems containing strut type elements. Limitations of passive damping are often characterized by static stiffness requirements and restrictions on the frequency dependence of damper properties. Active struts[5] that use materials such as piezoelectrics are normally capable of adding greater damping to a system and tailoring frequency dependence of the damping more easily. A purely active system, however, may require significant power and is subject to failure. A combination passive/active system reduces actuator power requirements and improves overall reliability while providing tailorable performance.

This paper examines one of several options for combining passive and active components for isolation or damping. One common approach to actively enhanced isolation makes use of voice coil actuation in parallel with a passive mount.[6] In contrast, the device discussed here uses an approach that involves hydraulic amplification of voice coil actuation. The same fluid also provides passive damping in strut or isolation devices. Viscous fluid damping and amplification has been used in elastomer (rubber) engine mounting designs for the past 20 years.[7]

The genesis of the device was a passive/active pneumatic strut[8] that used force actuation on a fluid bellows to pressurize a composite cylinder and worked well as a structural actuator. The viscous orifice damping, however, was very poor, and so work turned to transforming an existing viscous damper strut with proven damping performance. The original version of the D-strut® is used in an isolation system for the Hubble space telescope reaction wheel assembly.[2] More recently, modified versions of that isolation device have also been developed.[9] In addition, the viscous damper has been used in several controlled structures experiments to add damping to truss structures.[10] The new concept integrates a force actuator to pressurize the fluid in the damping cartridge of the D-strut. Figure 1 shows the passive damper with the actuator modifications.

This paper describes the design, analysis, and measured performance of a versatile device termed the AD-strut (active D-strut). The remainder of the paper begins with a derivation of

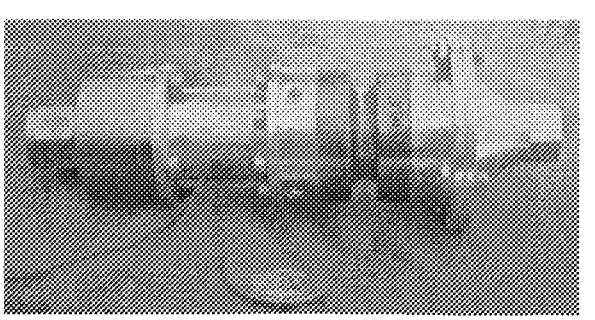

Fig. 1 Small voice coil AD-strut with collocated load cell.

Received April 12, 1995; revision received June 13, 1995; accepted for publication July 14, 1995.

*Graduate Research Assistant, Department of Aeronautics and Astronautics, Room 37-331, 77 Massachusetts Avenue. Member AIAA.

†Associate Principal Engineer, 2850 West Bayshore Road. Member AIAA.

a lumped parameter model that accurately represents the viscous damper/voice coil actuator combination. Next, component tests of the device are detailed. The results clearly show the effect of active augmentation. A series of experiments involving the use of the device as a truss member damper is then described. Performance using the actively enhanced passive damper compares favorably with that achieved using either passive viscous damping alone or active damping using a piezoelectric strut and local force feedback. Next, the same device is adapted for an isolation experiment. Results show significant reduction in force transmissibility when the combination passive/active isolation is employed.

Modeling of Prototype Device

Two versions of the AD-strut were fabricated and tested. One used a smaller voice coil force actuator than the other. The modeling for the large voice coil and small voice coil devices is identical. Later discussion of the experimental results notes the design that was used in each test.

The combination passive/active system is approximated well by a lumped parameter model. Any linear viscous damping mechanism can be modeled as a standard linear solid. Figure 2 shows the model that captures the stiffness and damping properties of the standard linear solid and accurately represents the passive operation of the device. At low frequency the dashpot c_A has no effect, and the element stiffness is k_A. At high frequency the dashpot stiffens, and the element stiffness approaches $k_A + k_B$. Damping is greatest in the frequency region of transition from low to high stiffness. The passive complex stiffness K can be written as a function of $s = j\omega$,

$$K(s) = (k_A + k_B)(s + w_z)/(s + w_p) \tag{1}$$

where

$$w_p = k_B/c_A = \alpha^2 w_z \tag{2}$$

$$w_z = k_A k_B/c_A(k_A + k_B) = w_p/\alpha^2 \tag{3}$$

$$\alpha^2 = (k_A + k_B)/k_A = 1 + (k_B/k_A) \tag{4}$$

The peak damping occurs at the log average of the pole and zero frequencies, and the peak loss factor depends only on the ratio of high to low frequency stiffnesses:

$$w^* = \sqrt{w_z w_p} = \alpha w_z \qquad \eta^* = (\alpha^2 - 1)/2\alpha \tag{5}$$

With the high- and low-frequency stiffnesses set, the peak damping frequency is selected by choosing c_A.

In the purely passive D-strut, a viscous fluid is compressed when the strut is loaded. The fluid flows through an orifice creating a pressure differential proportional to the fluid velocity. The disk of fluid that is compressed, termed the primary side fluid, is contained with an arch-shaped circular flexure. The fluid on the other end of the orifice tube, the secondary side fluid, is contained in a bellows type reservoir. An outer tube, inner tube, and end fitting stiffnesses (k_1, k_2, k_5) are also modeled. The linear damping from viscous flow through the orifice is modeled as a mechanical dashpot as shown in the more complicated model of the passive damper in Fig. 3. The parameters, their descriptions, and their specified values for the devices used are given in Table 1.

The fluid motion in the orifice exceeds the motion of the fluid leaving the primary side by the ratio of the area of the primary side disk to the area of the orifice. Similarly, the fluid motion on the secondary side is related to the orifice motion by another area ratio. These primary and secondary side area ratios are modeled mechanically as levers in Fig. 3. The orifice area can be reduced out of the model by arbitrarily setting the primary side area ratio to unity, thus leaving the secondary side lever ratio to be T (primary to secondary side area ratio). Note that for passive operation of the unmodified D-strut, the area ratio T and the secondary side parameters (k_6, k_7) are not important as long as k_6 is sufficiently smaller than k_3. The remaining parameters, k_1–k_5 and c, can be reduced to the three-parameter model of the standard linear solid.[10]

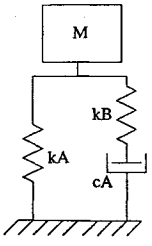

Fig. 2 Three-parameter model of D-strut; model accurately describes the passive behavior of the AD-strut.

Table 1 Lumped model parameters, their relative stiffnesses, their specification for the baseline D-struts, and the identified values from component tests of the large voice coil AD-strut

Parameter	Description	Ideal value	D-strut spec.	AD-strut meas.
k_1, N/μm	Outer tube	Soft/0	1.9	0
k_2, N/μm	Inner tube	Stiff	75	75
k_3, N/μm	Primary axial	Soft	1.4	1.81
k_4, N/μm	Primary radial	Stiff	75	41.9
k_5, N/μm	End fitting	Stiff	175	175
k_6, N/μm	Secondary axial	Soft	No spec.	0.018
k_7, N/μm	Secondary radial	Stiff	No spec.	0.35
k_m, N/μm	Preload and flexure	Soft	0.006	0.010
c, N$_s$/μm	Orifice dashpot	Variable	0.026	0.030
T	Area lever ratio	Variable	No spec.	6.93

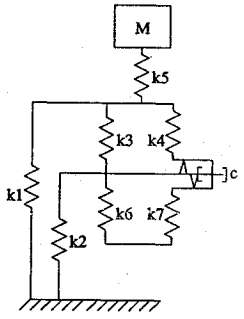

Fig. 3 Lumped parameter model of the unmodified D-strut showing area ratio lever and dashpot model of fluid orifice.

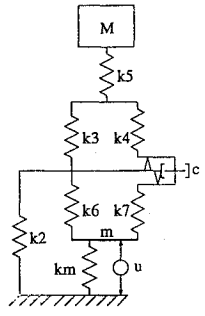

Fig. 4 Lumped parameter model of AD-strut including voice coil force actuator on secondary side of fluid orifice.

Figure 4 shows the AD-strut model. It includes several changes from the ordinary D-strut model of Fig. 3. The outer tube, modeled by k_1, was removed since it served only to modify the low-frequency stiffness and was not needed in the AD-strut. The inner tube, modeled by k_2, was replaced by a new inner tube that also holds the voice coil magnet and casing. Finally, the voice coil moving element (mass m) was attached to the secondary side, providing a force between the base and the fluid reservoir. With no power to the actuator, the only modification to the original D-strut was the removal of k_1 and the addition of k_m, the voice coil motor flexure stiffness. The last column of Table 1 gives the values of the parameters for the large voice coil AD-strut as measured by component tests. The small voice coil version is shown in Fig. 5. In summary, modifications to the D-strut were the removal of the outer tube, the replacement of the inner tube to mate to the motor casing, and the attachment of the plastic voice coil moving element to the end of the bellows. The voice coil leads exit through a small hole drilled in the side of the new inner tube. No flexures are needed ($k_m = 0$) since the weight of the small plastic voice coil is only 5 g. The earlier large voice coil AD-strut needed flexures made of rubber strips to hold the heavier aluminum voice coil and to prevent it from rubbing the inside of the motor casing.

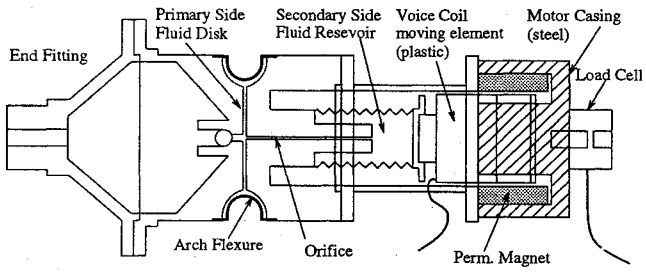

Fig. 5 Assembly drawing of small voice coil AD-strut, total length 12 cm and total mass 220 g.

A state space model of the AD-strut was constructed based on the mechanical model of Fig. 4. The states are the velocity and position of the spring junctions and the position of the fluid in the orifice. The mass of most spring junctions is set to an infinitesimal value, and the model is reduced mathematically. The payload mass M and the voice coil mass m are retained, resulting in a five-state system. This system was used to evaluate passive and active transfer functions from the AD-strut command u and from an external force on M.

Device Characterization

Several component-level tests were conducted to fully characterize passive and active performance of the AD-strut and verify the analytical model. Passive complex stiffness, blocked force, and free stroke transfer functions were measured and used to update the lumped parameter model.

Test Setup

The single-axis component test fixture (Fig. 6) characterizing active and passive struts consisted of two steel blocks bolted to an optics bench with a Physik Instrumente P-243.40 piezoelectric driver, a PCB 208A load cell, and a laser interferometeric displacement measurement (Zygo Axiom 2/20) in line with the strut to be tested. For measurement of passive complex stiffness, the strut was placed in the component tester as shown in Fig. 6, and the piezoelectric driver applied a force with sinusoidal or white noise characteristics. The transfer function from displacement to load was recorded by a spectrum analyzer. The blocked force of an active strut was measured without reconfiguring the test fixture; the stiff piezoelectric driver was shut off and the active strut was driven with a sinusoidal or white noise signal. The load cell measured the blocked force output of the active strut as a function of the strut command input. The connector rods of the component tester were removed to measure the free stroke of an active strut. The laser metrology system then measured the free displacement as a function of strut command input.

Component Level Test Results

The motor constant was evaluated by placing the voice coil alone in the blocked force measurement configuration and was found to be 6.8 N/A. Next, the entire passive/active device was placed in the component tester, and passive complex stiffness (Fig. 7) was measured. Structural modes of the optical bench are observable above about 80 Hz. The AD-strut has a static stiffness of 2.8 N/μm and peak loss factor of 1.2 (corresponding to 50 deg of phase) at about 50 Hz. The zero and pole frequencies were found with a curve fit to be 15 and 130 Hz, respectively. Linearity of the device is demonstrated by the nearly identical transfer function measured at two different forcing levels.

With the piezoelectric driver off, the AD-strut was excited with a white noise driving signal. The transfer function from motor current to blocked force is shown in Fig. 8. The tests were done at several forcing levels and showed good linearity. The low-frequency blocked force is 34 N/A and the corner frequency of the viscous orifice damping is about 55 Hz. This rolloff is due to internal compliances and the finite stiffness of the test fixture (22 N/μm). If the strut were ideally blocked, the observed rolloff would be at a higher frequency.

Finally, the AD-strut was placed in the free displacement configuration and the transfer function recorded from motor current to measured displacement. Figure 9 shows these free stroke results for two forcing levels. The low-frequency free stroke is 12 μm/A and the rolloff from the viscous orifice damping shows up at about 15 Hz (the frequency of the zero in the complex stiffness measurement).

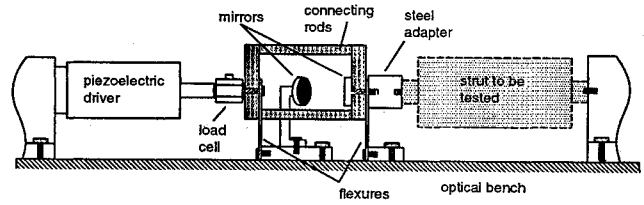

Fig. 6 Drawing of component tester showing force and displacement measurements.

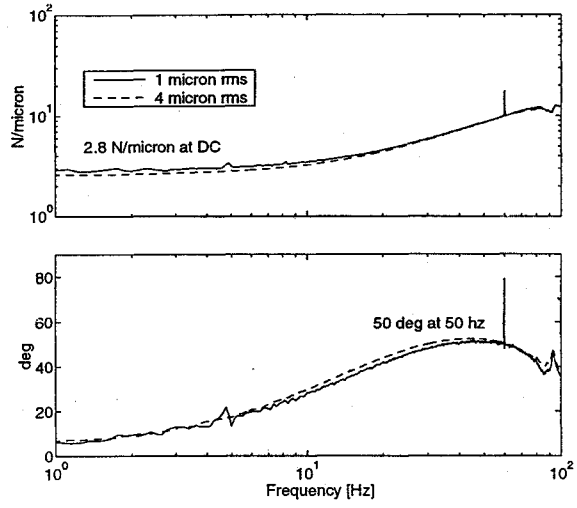

Fig. 7 Measured AD-strut passive complex stiffness shown for two forcing levels; peak loss factor 1.2 near 50 Hz.

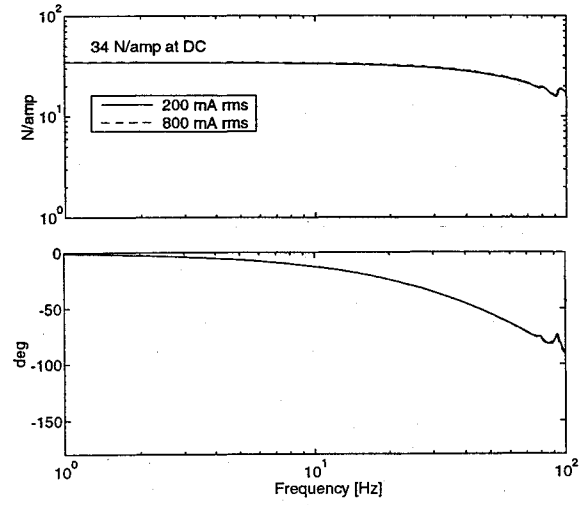

Fig. 8 AD-strut control current to blocked force transfer functions for two input forcing levels.

Update of Model Parameters

The lumped model parameters of Table 1 were updated using the information obtained in component tests. Since several of the stiffnesses are not identifiable independently, k_2 (the inner tube) and k_5 (the end fitting) were fixed to be the values specified in the D-strut design. The flexure stiffness k_m was measured directly, and the secondary radial stiffness k_7 was measured by observing the high-frequency resonance of the moving coil mass. Four other parameters were measured: the low-frequency passive stiffness, the high-frequency passive stiffness, the low-frequency free stroke, and the low-frequency blocked force. The four unknowns (k_3, k_4, k_6, and T) were found by a simple gradient search optimization that

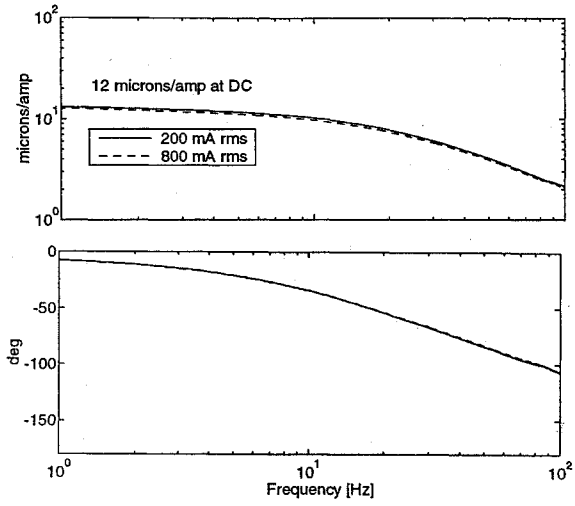

Fig. 9 Measured AD-strut control current to free stroke transfer functions for two input forcing levels.

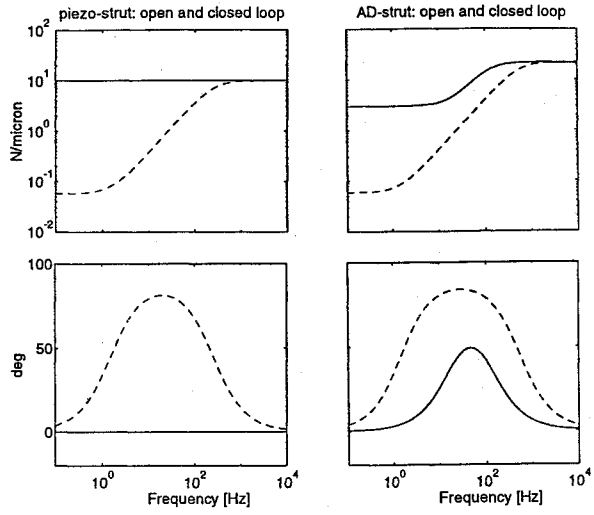

Fig. 10 Complex stiffnesses of piezoelectric strut and AD-strut for passive (solid line) and active (dashed line) damping.

fitted model stiffnesses and dc gains to the measured values. Once the unknown parameters were determined, the peak damping frequency and the rolloff in free stroke were set by c. Results of the fit are shown in the last column of Table 1. The AD-strut properties were used in prediciting performance for two applications, damping and isolation.

Active/Passive Damping Experiments

Several structural damping experiments were conducted on a truss testbed. This structurally complex scale model of a future space-based interferometer is used for research in structural control and identification, optical pathlength control, and passive and active damping.[11] The AD-strut was compared to two standard approaches for strut-based damping augmentation: a viscous passive damper (an unmodified D-strut) and an active piezoelectric strut with local force feedback.[5]

Demonstration of Complex Stiffness Modification

A comparison of the damping operation of a piezoelectric active strut and the new device is easily quantified by measurement of complex stiffness. A passive piezoelectric strut has little inherent damping. Active damping is achieved by feeding back collocated integral load to the piezoelectric actuator. The strut is effectively destiffened at low frequencies, and the stiffness increases with frequency as the integral control rolls off. Damping is present in the range where the stiffness is increasing, as seen in the phase of the complex stiffness. Figure 10 shows the complex stiffness of a piezoelectric strut passively (about 10 N/μm) and actively damped, with feedback integration stabilized at 1.3 Hz. Integral force feedback (IFF) yields broadband damping centered in the frequency range of interest (10–80 Hz).

In the case of the AD-strut, passive damping is achieved through viscous forces in the D-strut cartridge as outlined earlier. Figure 10 shows the familiar complex stiffness of the three-parameter model with the damping present in the region of increasing stiffness. Actively damped, the AD-strut is used with force feedback to destiffen the strut at low frequency. In this way, the closed-loop AD-strut is very similar to the closed-loop piezoelectric strut. Notice that the closed-loop complex stiffnesses of both struts are virtually the same. The AD-strut has a greater high-frequency stiffness, yielding slightly broader damping for the same gain, while retaining the damping characteristics of a passive D-strut when the control is turned off.

Test Setup

Figure 11 shows a drawing of the Massachusetts Institute of Technology tetrahedral-shaped trusswork testbed structure; each leg is 3.5 m long. A laser metrology system measures the performance metric: the differential optical path length from the three siderostats, A, B, C, to the combining optics location, E. Three proof mass

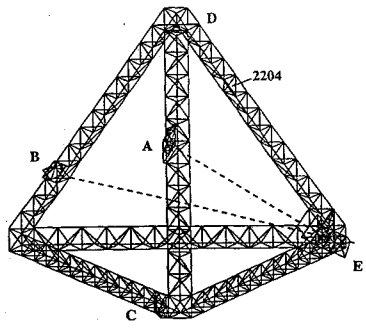

Fig. 11 Interferometer testbed showing damping strut (2204), disturbance (D), and optical path lengths (AE, BE).

shakers at location D represent an onboard vibration source. Using a finite element model of the testbed,[3] strut location 2204 was chosen as a high-strain location affecting the disturbance to differential AB laser measurement. The AD-strut, an unmodified D-strut, and a piezoelectric strut were used to replace the normal aluminum tube strut in this location to add damping and reduce the differential AB rms motion. For reference, disturbance to performance data was first taken on the unmodified testbed. Note that this testbed includes 50 strategically distributed constrained layer viscoelastic damper struts. The mode at 53 Hz, with modal damping ratio $\zeta = 0.008$ was identified as the main contributor to performance and was the target of the active damping controllers.

Test Results

Testing consisted of replacing the nominal aluminum strut in location 2204 with an unmodified D-strut, a piezoelectric strut, and the AD-strut. In each case the damping in the mode near 53 Hz and the rms of the differential AB laser displacement is reported (Table 2).

The unmodified D-strut (see Fig. 12), designed for this testbed with peak damping set around 60 Hz, yielded a damping of 1.5% for the 53-Hz mode, lowering the performance rms from 123 to 102 nm (10–80 Hz). The dash–dot curves in Fig. 13 show disturbance to performance transfer function data for the unmodified D-strut.

The piezoelectric strut (Physik Instrumente type P-843.20) with collocated load cell (PCB 208B) was placed in location 2204 and data taken as before (see Fig. 14). With no control, the damping and rms were unchanged from that of the aluminum strut test. With the IFF loop closed and the gain adjusted to minimize differential AB rms, the 53-Hz mode was damped to 4.1% and the 10–80 Hz rms reduced to 85 nm. The solid curves in Fig. 13 show the open- and closed-loop disturbance to performance transfer function data

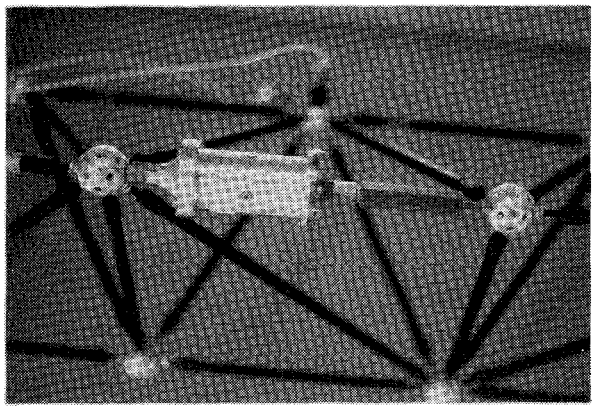

Fig. 12 Unmodified passive D-strut used in damping experiments.

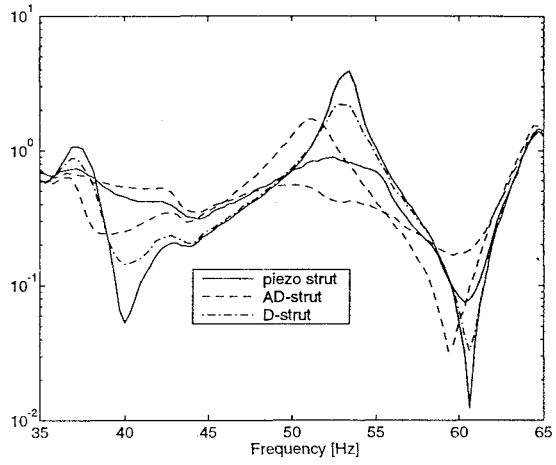

Fig. 13 Disturbance to performance transfer functions for piezo strut open- and closed-loop (solid line), AD-strut open- and closed-loop (dashed line), and D-strut (dash–dot line).

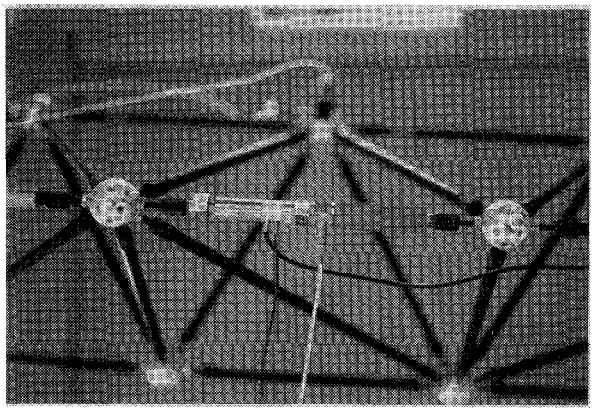

Fig. 14 Piezoelectric active strut used in damping experiments.

for the piezoelectric strut. Various other local control strategies for active damping using piezoelectric struts in experiments on the same testbed are reported elsewhere.[3,12,13]

The AD-strut was then inserted in location 2204; the photograph of Fig. 15 shows the placement with collocated load cell (PCB 208B). With no power applied to the strut, the 53-Hz mode was damped to 2.0% and shifted down in frequency to 51 Hz due to the added mass of the large voice coil AD-strut. The resulting laser rms motion was 91 nm at 10–80 Hz. An IFF control was then closed, lowering the low-frequency stiffness similar to the piezoelectric strut control. A one pole analog lead filter was used with the integrator; the zero and pole were set at 15 and 130 Hz, respectively, to invert the pole and zero of the passive AD-strut. A notch filter was used to invert the internal resonance associated with the mass of the large voice coil. With the inherent dynamics of the D-strut inverted, the closed-loop AD-strut mimicked the closed-loop piezoelectric strut. With loop

Table 2 Truss damping results for various struts

Strut	rms motion (AB, 10–80 Hz), nm	Primary mode damping, %
Nominal aluminum strut	123	0.8
Unmodified D-strut	102	1.5
Passive piezoelectric strut	123	0.8
Active piezoelectric strut	85	4.1
Passive AD-strut	91	2.0
Active AD-strut	83	8.8

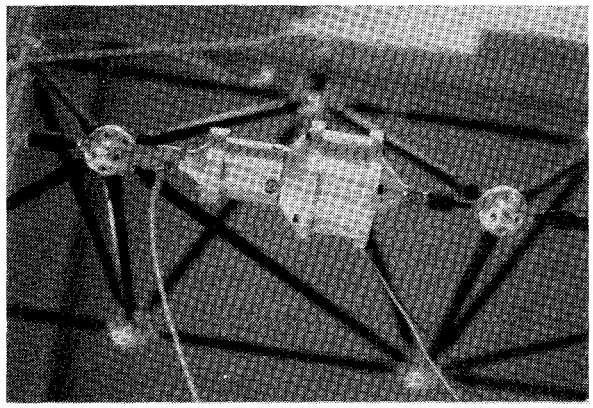

Fig. 15 Large voice coil AD-strut used in damping experiments.

gain adjusted for best differential AB rms, the AD-strut with load cell feedback damped the 53-Hz (now 51) mode to 8.8%, yielding 83-nm rms 10–80 Hz. The dashed curves in Fig. 13 show the open- and closed-loop disturbance to performance transfer function data for the AD-strut.

Summary of Damping Results

For structural damping, the AD-strut performs as well or better than a regular D-strut damped passively and as well or better than a piezoelectric strut damped actively using load cell feedback (Table 2). The obvious advantage of the AD-strut is that the passive damping is present even when no control is used.

Force Isolation Experiments

The other major application of this active viscous strut (and the prime motivation for its development) is passive/active vibration isolation. An experimental apparatus was constructed to test the AD-strut for single-axis force isolation. As with the damping experiments, the approach was to demonstrate performance with the passive viscous system, then show the additional improvement achievable with active enhancement.

Test Setup

A rigid mass (30-kg steel block) modeled the isolated equipment, and a proof-mass shaker (B&K Type 4809) provided the disturbance force; both were suspended by 50-cm cables. In three separate experiments, an undamped steel strut, an unmodified D-strut, or the AD-strut were used to attach the mass to the wall. Figure 16 shows the layout of these elements along an axis perpendicular to gravity. Two load cells (PCB 208B) were used: one to measure the input disturbance force and one to measure the force transmitted to the wall. The mount transmissibility is the magnitude of the transfer function from disturbance to wall load measurements. The wall load cell was also used as a feedback error sensor for active control of the AD-strut. A steel wire stinger was inserted between shaker and mass, and a turned down steel rod flexure was used between strut and wall to reduce excitation or measurement of off-axis loads. An aluminum plate (2.5 cm thick) was bolted to the cinderblock wall and appeared to provide a rigid base in the frequency range of interest, but wall (base) modes can be seen in the measured transfer functions around 60 and 130 Hz.

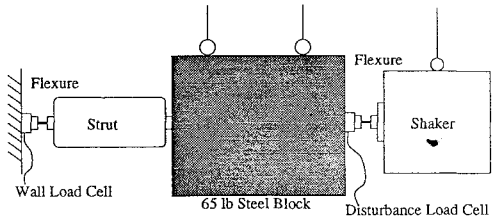

Fig. 16 Experimental setup for force isolation; transmissibility is the disturbance force to wall force transfer function.

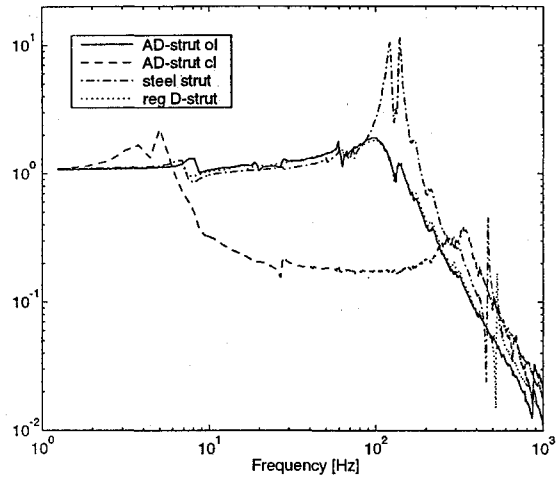

Fig. 17 Transmissibility for AD-strut open (solid line) and closed-loop (dashed line), unmodified D-strut (dotted line), and steel strut (dash–dot line).

Passive Isolation

The resonant frequency of the mass on an unmodified D-strut was 97 Hz with a damping ratio of 31%. The compliance of the flexure, wall, and other hardware in the load path reduced the effective series stiffness k_5, causing a reduced high-frequency stiffness and peak damping. The measured transmissibility is unity below mount resonance and exhibits the expected second-order rolloff (−40 dB/decade) above mount resonance. The rms of the wall force was measured (0–1000 Hz) to be 1.32 N. The AD-strut with no control was found to almost exactly match the transmissibility of the unmodified D-strut, as expected, with a resulting wall force 1.25-N rms. For comparison, an undamped steel rod (14 cm long, 2.5 cm diameter) was also tested. Again, due to the series stiffness in the setup and wall resonance, the steel rod exhibited a double mount resonance at 120 and 150 Hz with little damping and yielded a wall force of 3.30-N rms. Figure 17 shows these three passive transmissibilities.

Active Isolation

Active control of the AD-strut isolation mount was accomplished with feedback of the wall load cell measurement. The plant transfer function from commanded voice coil current to feedback sensor was measured using a Tektronix 2641 spectrum analyzer and random input. These data, along with disturbance force to wall force data, were used in a two-input/one-output system identification. The resulting model was then augmented with a one-pole Padé approximation to a pure time delay representing the 5330-Hz sample rate of the digital computer used for control. A compensator was designed using the linear quadratic Gaussian (LQG) control methodology[14] with control and performance frequency weightings. The resulting 12 state compensator was Tustin transformed to discrete time and implemented on a VME-based real-time computer.

Figure 17 shows the active AD-strut mount transmissibility with improvement over that of the open-loop mount in the range of 6–250 Hz. Note that the effective mount resonance has been moved down in frequency to just above 4 Hz. Transmitted force at the wall was reduced to 0.33-N rms, an 11.6-dB improvement over the passive mount, and a 20-dB improvement over the undamped steel mount. Additional performance was limited by the need to roll off the loop gain in the region around 300 Hz due to phase lags caused by the computer time delay and the rolloff required to gain stabilize high-frequency plant resonances around 3500 Hz.

Summary of Isolation Results

For isolation, the AD-strut with active control turned off performed as well as a passive viscous isolator. The mount resonance was reduced by more than a decade when load cell feedback was added. Active enhancement of the passive device improved the broadband force isolation performance from 8.4 to 20 dB with respect to an undamped mount. One obvious advantage of the actively enhanced passive system is that the passive isolation is present even when no control is used.

Conclusions

A novel actuator with built-in viscous damping for vibration isolation and structural control has been developed, modeled, tested, and applied. The device builds on the excellent passive damping properties of a viscous damper cartridge. By using a force actuator through the fluid lever of an area ratio, better force and stroke properties were attained compared to those possible for a force actuator in parallel with the passive element. The tradeoff for this force amplification is an inherent rolloff in the actuation authority as the fluid orifice locks up at high frequency. This rolloff is not a problem in most applications where loop gain rolls off at high frequency anyway. The AD-strut is well suited for vibration isolation and structural control applications in which the passive stiffness and damping are insufficient to meet requirements.

For vibration isolation, the passive element is built to support the isolated equipment with minimum gravity sag and moderate damping. For better isolation (e.g., when sensitive instruments are operating), active control using load cell or accelerometer feedback can be applied to lower the mount resonant frequency by more than a decade. Experiments with single-axis isolation using the AD-strut demonstrated an 8-dB passive and 20-dB active improvement over an undamped mount. Narrow-band isolation could also be implemented for rejecting sinusoidal disturbances.

For structural control, the passive element is built for required stiffness and provides a good level of passive damping. The active element provides improved broadband damping performance using feedback of local sensor information. Low authority control strategies such as integral force feedback are well suited for improving broadband damping. In a truss testbed, the AD-strut demonstrated the passive damping performance of an unmodified passive damper and the active performance of a piezoelectric strut with IFF control. Compared to a piezoelectric strut, the AD-strut has the advantage of using smaller control voltages, reducing the need for heavy power electronics.

The ultimate advantage of this new actuator with built-in viscous damping is that even when the active control is turned off (or fails), appropriate passive stiffness and damping are still present. This property is key in spacecraft applications, since the device can be unpowered for launch, yet still provide some isolation and damping to protect sensitive equipment during launch transients. The active control is then turned on during operations for improved isolation and damping performance. The force actuator required is many times smaller than that required for a parallel arrangement, resulting in weight and power savings.

Acknowledgments

This research was supported by NASA Grant NaGW-1335. The authors acknowledge David Penner and Sherwin Chen for their help in building and testing the actuators.

References

[1]Crede, C. E., "Theory of Vibration Isolation," *Shock and Vibration Handbook*, edited by C. M. Harris, McGraw–Hill, New York, 1961, Chap. 30.

[2]Wilson, J. F., and Davis, L. P., "Viscous Damped Space Structure for Reduced Jitter," 58th Shock and Vibration Symposium, Oct. 1987.

[3]Anderson, E. H., "Robust Placement of Actuators and Dampers for Structural Control," Ph.D. Thesis, Massachusetts Inst. of Technology, Cambridge, MA, Oct. 1993.

[4]Von Flotow, A. H., "An Expository Overview of Active Control of Machinery Mounts," *Proceedings of the 27th Conference on Decision and Control* (Austin, TX), Inst. of Electrical and Electronics Engineers, New York, 1988.

[5]Preumont, A., Dufour, J. P., and Malekian, C., "Active Damping by a Local Force Feedback with Piezoelectric Actuators," *Journal of Guidance Control, and Dynamics*, Vol. 15, No. 2, 1992, pp. 390–395.

[6]Spanos, J., Rahman, Z., and von Flotow, A., "Active Vibration Isolation on an Experimental Flexible Structure," *SPIE Proceedings*, Vol. 1917, 1993, pp. 674–680.

[7]Flower, W. C., "Understanding Hydraulic Mounts for Improved Vehicle Noise, Vibration and Ride Qualities," Surface Vehicle Noise and Vibration Conf., Traverse City, MI, 1985.

[8]Ciero, M. K., "Design of a Fluid Elastic Actuator with Application to Structural Control," M.S. Thesis, Massachusetts Inst. of Technology, Cambridge, MA, May 1993.

[9]Davis, L. P., Cunningham, D., Bicos, A. S., and Enright, M., "Adaptable Passive Viscous Damper: an Adaptable D-strut," *SPIE Proceedings*, Vol. 2193, 1994, pp. 47–58.

[10]Anderson, E. H., Trubert, M., Fanson, J. L., and Davis, L. P., "Testing and Application of a Viscous Passive Damper for Use in Precision Truss Structures," *Proceedings of the AIAA Structures, Structural Dynamics, and Materials Conference*, AIAA, Washington, DC, 1991, pp. 2796–2808.

[11]Blackwood, G. H., Miller, D., and Jacques, R., "The MIT Multipoint Alignment Testbed: Technology Development for Optical Interferometry," *SPIE Proceedings*, Vol. 1542, 1991, pp. 371–391.

[12]Anderson, E. H., Blackwood, G. H., and How, J. P., "Passive Damping in the MIT SERC Controlled Structures Testbed," Active Materials and Adaptive Structures Conf., Alexandria, VA, Nov. 1991.

[13]Spangler, R. S, "Broadband Control of Structural Vibration Using Simultaneous Sensing and Actuation with Nonlinear Piezoelectric Elements," Ph.D. Thesis, Massachusetts Inst. of Technology, Cambridge, MA, Dec. 1993.

[14]Gupta, N. K., "Frequency-Shaped Cost Functionals: Extension of Linear Quadratic Guassian Design Methods," *Journal of Guidance and Control*, Vol. 3, No. 6, 1980, pp. 529–535.